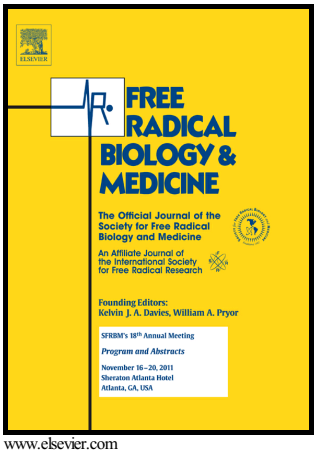

www.elsevier.com

OXIDATIVE STRESS DAMAGE CIRCUMSCRIBED TO THE CENTRAL TEMPORAL RETINAL PIGMENT EPITHELIUM IN EARLY EXPERIMENTAL NON-EXUDATIVE AGE-RELATED MACULAR DEGENERATION

Hernán H. Dieguez, Horacio E. Romeo, Agustina Alaimo, María F. González Fleitas, Marcos L. Aranda, Ruth E. Rosenstein, Damián Dorfman

PII: S0891-5849(18)31760-X
DOI: https://doi.org/10.1016/j.freeradbiomed.2018.11.035
Reference: FRB14057

To appear in: *Free Radical Biology and Medicine*

Received date: 3 October 2018
Revised date: 27 November 2018
Accepted date: 27 November 2018

Cite this article as: Hernán H. Dieguez, Horacio E. Romeo, Agustina Alaimo, María F. González Fleitas, Marcos L. Aranda, Ruth E. Rosenstein and Damián Dorfman, OXIDATIVE STRESS DAMAGE CIRCUMSCRIBED TO THE CENTRAL TEMPORAL RETINAL PIGMENT EPITHELIUM IN EARLY EXPERIMENTAL NON-EXUDATIVE AGE-RELATED MACULAR DEGENERATION, *Free Radical Biology and Medicine,* https://doi.org/10.1016/j.freeradbiomed.2018.11.035

OXIDATIVE STRESS DAMAGE CIRCUMSCRIBED TO THE CENTRAL TEMPORAL RETINAL PIGMENT EPITHELIUM IN EARLY EXPERIMENTAL NON-EXUDATIVE AGE-RELATED MACULAR DEGENERATION

Hernán H. Dieguez[a], Horacio E. Romeo[b], Agustina Alaimo[c], María F. González Fleitas[a], Marcos L. Aranda[a], Ruth E. Rosenstein[a1], Damián Dorfman[a1*]

[a]Laboratory of Retinal Neurochemistry and Experimental Ophthalmology, Department of Human Biochemistry, School of Medicine/CEFyBO, University of Buenos Aires/CONICET, Buenos Aires, Argentina

[b]School of Engineering and Agrarian Sciences, Pontifical Catholic University of Argentina, BIOMED/UCA/CONICET, Buenos Aires, Argentina

[c]Interdisciplinary Laboratory of Cellular Dynamics and Nanotools, Department of Biological Chemistry, Faculty of Exact and Natural Sciences/IQUIBICEN, University of Buenos Aires/CONICET, Buenos Aires

[*]Corresponding author: Dr. Damián Dorfman, Departamento de Bioquímica Humana, Facultad de Medicina/CEFyBO, UBA/CONICET, Paraguay 2155, 5º P, (1121), Buenos Aires, ARGENTINA, Phone n°: 54-11-4508-3672 (ext. 37), FAX n°: 54-11-4508-3672 (ext. 31), ddorfman@fmed.uba.ar

ABSTRACT:

Non-exudative age-related macular degeneration (NE-AMD) represents the leading cause of blindness in the elderly. The macular retinal pigment epithelium (RPE) lies in a high oxidative environment because its high metabolic demand, mitochondria concentration, reactive oxygen species levels, and macular blood flow. It has been suggested that oxidative stress-induced damage to the RPE plays a key role in NE-AMD pathogenesis. The fact that the disease limits to the macular region raises the question as to why this area is particularly susceptible. We have developed a NE-AMD model induced by superior cervical ganglionectomy (SCGx) in C57BL/6J mice, which reproduces the disease hallmarks exclusively circumscribed to the temporal region of the RPE/outer retina. The aim of this work was analyzing RPE regional differences that could

[1] Both authors contributed equally to this work.

explain AMD localized susceptibility. Lower melanin content, thicker basal infoldings, higher mitochondrial mass, and higher levels of antioxidant enzymes, were found in the temporal RPE compared with the nasal region. Moreover, SCGx induced a decrease in the antioxidant system, and in mitochondria mass, as well as an increase in mitochondria superoxide, lipid peroxidation products, nuclear Nrf2 and heme oxygenase-1 levels, and in the occurrence of damaged mitochondria exclusively at the temporal RPE. These findings suggest that despite the well-known differences between the human and mouse retina, it might not be NE-AMD pathophysiology which conditions the localization of the disease, but the macular RPE histologic and metabolic specific attributes that make it more susceptible to choroid alterations leading initially to a localized RPE dysfunction/damage, and secondarily to macular degeneration.

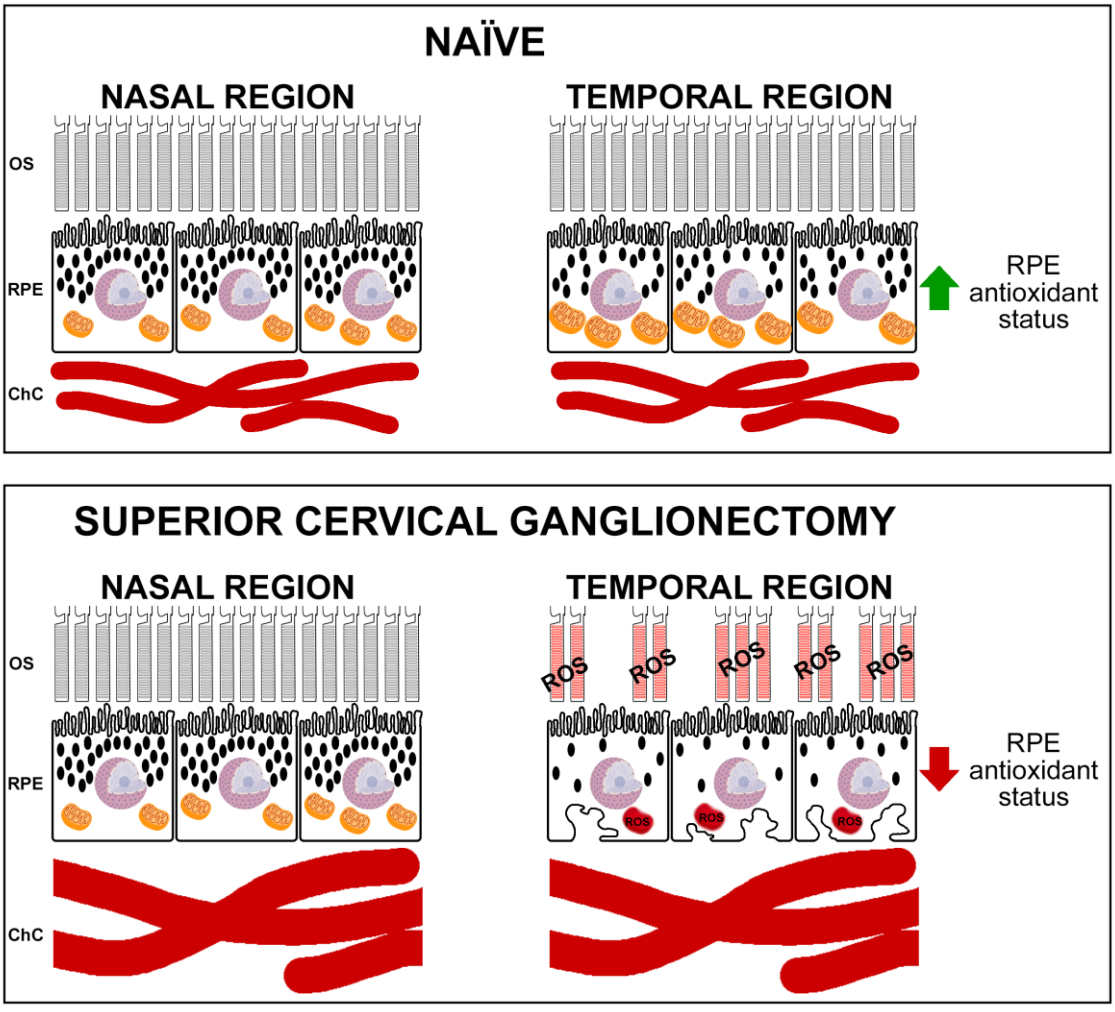

OS: photoreceptor outer segments; RPE: retinal pigment epithelium; ChC: choroid/choriocapillaris; ROS: reactive oxygen species

Keywords:

non-exudative age-related macular degeneration, superior cervical ganglion, retinal pigment epithelium, oxidative stress, mitochondria, antioxidant system.

STATEMENT

Non-exudative age-related macular degeneration (NE-AMD) is a leading and presently untreatable cause of blindness in the elderly. One of the most striking characteristics of the disease is that, even at final stages, only the central retina (i.e., the macula) is damaged, while the rest of the retina remains unaltered, which raises the question as to why this area is particularly susceptible to the disease. Using a mouse experimental model induced by choroid vascular alterations, we found that there are structural, biochemical, and mitochondrial differences between the central and non-central retinal pigment epithelium (RPE), which support that it might not be NE-AMD etiopathogenesis, but the macular RPE histologic and metabolic specific attributes that make it more susceptible to NE-AMD induced damage

INTRODUCTION

Age-related macular degeneration (AMD), a leading cause of irreversible blindness in elders, is a chronic progressive disease affecting central vision, with an estimate prevalence of ~ 9% of the global population (Datta et al., 2017, Wong et al., 2014). AMD can be classified in two forms: exudative, and non-exudative. Non-exudative AMD (NE-AMD) is characterized by the progressive atrophy of the macular retinal pigment epithelium (RPE) and photoreceptors, and accounts for ~ 80% of all intermediate and advanced forms of the disease (Buschini et al., 2015). The advanced form of NE-AMD is termed geographic atrophy (GA) due to its precise atrophic limit, and is characterized by the breakdown of the RPE, choriocapillaris, and macular

photoreceptors, leading to severe and irreversible central vision loss. At the moment, there are no therapies to restore the vision loss in patients with advanced NE-AMD.

AMD is a multi-factorial disease; several risk factors such as age, female sex, cigarette smoking, diet, and Caucassian race have been associated with the developing and progression of AMD (Datta et al., 2017; Lambert et al., 2016; van Lookeren Campagne et al., 2014). In addition, RPE lipofuscin accumulation, choroidal blood flow insufficiency, inflammation, and oxidative stress have been involved in NE-AMD etiopathogenesis (Bowes Rickman et al., 2013; Ding et al., 2009; Zarbin, 2004). Different studies indicate that damage to the RPE is an early event in AMD (Ach et al., 2015; Cai et al., 2000; Datta et al 2017), and clinically and experimentally relevant AMD results support that damage to the RPE is mainly caused by oxidative stress (Lambros and Plafker, 2016; Mao et al., 2014; Sachdeva et al., 2014; Zarbin, 2004). The macula lies in a high oxidative environment in part, because the RPE has a high metabolic demand that generates high levels of reactive oxygen species (ROS) produced from cellular metabolism to meet its multiple functions, and in part because of the macular blood flow (one of the highest in the body), and the high local oxygen partial pressure (i.e., between 70 - 90 mm Hg) (Datta et al., 2017; Winkler et al., 1999). Due to its high metabolic activity, the RPE is enriched with mitochondria, which are a major source of ROS in the RPE (Jager et al., 2008). The observation that the disease is circumscribed to the macular area, raises the question as to why the macula is particularly susceptible to the disease, while the rest of the retina remains (at least clinically) unaltered. Although there are no definitive answers to this question partly because the available animal models do not recapitulate this particular characteristic of the disease, the explanation is likely to be related to both the metabolic and structural attributes of this particular retinal region that differ from its surroundings, and to the functional alterations induced by the disease itself. A main problem in modelling NE-AMD in mice (the most frequent animal model for AMD) is that their retina lacks a macula. However, new evidence may argue on this point, since a central area

with a highest cone concentration, human-like cone/rod ratio, and Bruch´s membrane (BrM), and RPE specialization was described in C57BL/6J mice (Volland et al., 2015). Recently, we have developed an experimental model of NE-AMD induced by superior cervical ganglionectomy (SCGx) in C57BL/6J mice (Dieguez et al., 2018). In that context, we have shown that SCGx induces a photoreceptor function decline, and ubiquitous choroid and choriocapillaris changes, whereas BrM thickening, RPE melanin content, and retinoid isomerohydrolase loss, drusen-like deposit occurrence, and RPE and photoreceptors atrophy are exclusively localized in the temporal side of the optic nerve. Moreover, SCGx provokes RPE and photoreceptors apoptosis also localized in the temporal region. Therefore, unlike all the others experimental (genetically engineered, immunologically manipulated or mouse strains with spontaneously arising retinal degeneration) models of AMD, SCGx-induced NE-AMD has the clear advantage of inducing AMD-like alterations circumscribed to a particular region, corresponding to the mouse central retina described by Volland et al. (2015). Identifying the mechanisms that make only the temporal side sensitive to the SCGx-induced NE-AMD damage could contribute to understand the particular susceptibility of the human macula to AMD. In that context, the aim of this work was to analyse comparatively the mitochondrial status and the endogenous antioxidant system in the nasal and temporal RPE from naïve mice, and evaluating the involvement of oxidative stress in the temporal RPE/neural retina damage induced by SCGx.

MATERIAL AND METHODS

Animals

All animal use procedures were in strict accordance with the NIH Guide for Care and Use of Laboratory Animals. The ethics committee of the University of Buenos Aires School of Medicine, (Institutional Committee for the Care and Use of Laboratory Animals, (CICUAL)) approved this study). Adult male C57BL/6J mice (average weight, 27 ± 3 g and average age 2.5

± 0.5 months) were housed in a standard animal room with food and water *ad libitum*, under controlled conditions of humidity and temperature (21 ± 2°C). The room was lighted by fluorescent lights (200 lux), which were turned on and off automatically every 12 hours (on from 8.00 AM to 8.00 PM). For all experimental procedures, animals were anesthetized with intramuscular injection of 100 mg/kg ketamine hydrochloride and 1 mg/kg xylazine hydrochloride.

RPE melanin content quantification

Mice were intracardially perfused with 0.1 M PBS, pH 7.4, containing 0.5 ml heparin and 2.4% sodium nitroprusside as vasodilator, followed by a fixative solution containing 4% formaldehyde. Naïve eyes were carefully removed; the nictitating membrane was left attached to the eye for orientating purposes. After dehydration, samples were embedded in paraffin wax, transverse sections (5 μm) across the optic nerve head (ONH) were obtained with a microtome (2125 RTS, Leica Biosystems, Buenos Aires, Argentina), and after deparaffinisation and dehydration were mounted in Canada balsam without any other treatment, in order to avoid any interference in the final result. Light microscopic images (×1000) were digitally captured, and analysed by masked observers. For each eye, the pigment area only present in the central nasal and temporal RPE at exactly 800 μm from the ONH was quantified using ImageJ software version 1.42q (NIH, Bethesda, MD), and the average from four separate sections per eye (in the superior-inferior axis), and the mean of 5 eyes was recorded as the representative value for each group.

Electron microscopy

Mice were intracardially perfused using an *ad hoc* pump with 0.1 M PBS, pH 7.4, containing 0.5 ml heparin and 2.4% sodium nitroprusside, followed by a fixative solution containing 2%

glutaraldehyde and 4% formaldehyde. Eyecups were sectioned along the horizontal meridian (nasal-temporal axis) through the optic nerve, and post-fixed with 1% osmium tetroxide for 2 hours on ice. Samples were embedded in epoxy resin. Ultrathin sections (50 nm) from the central nasal and temporal RPE (at 800 μm from the ONH) were obtained using glass knives and an ultramicrotome Ultracut E (Reichert-Jung, Vienna, Austria). Sections were mounted on 300 Mesh grids and stained with uranyl acetate (2% in 70% ethanol) and Reynolds lead citrate. Finally, sections were viewed and photographed using a Zeiss 109T transmission electron microscope (Carl Zeiss Microscopy, Peabody, MA, USA), equipped with a digital camera (ES1000W, Gatan, Pleasanton, CA, USA). Melanin granules and basal infoldings thickness were measured. For each group, 5 different sections from 4 different samples were averaged and the mean taken as the representative value. The area occupied by mitochondria in 100 μm^2 was quantified using ImageJ software version 1.42q (NIH, Bethesda, MD), and only mitochondria with distinguishable outer and inner membranes were evaluated. For each group, ultraphotomicrographs from 3 eyes were analysed.

Tissue harvesting for SDS-PAGE and Western blotting

After cervical dislocation, eyes were enucleated and the cornea and lens removed. Whole flat-mounts (i.e., containing the retina and RPE) were placed on an iced dish, where a vertical incision across the ONH was done under a surgical microscope, thus obtaining the nasal and temporal hemi-retina/RPE. Finally, the neural retina was carefully detached from the RPE, and both tissues were homogenized as described below. In order to ensure that RPE preparation was not contaminated with the neural retina and *vice versa*, an analysis of retinoid isomerohydrolase (RPE65) and visual arrestin protein levels were performed in these samples by Western blot. As shown in Figure S1, RPE65 was only present in RPE homogenates, whereas visual arrestin was

predominantly present in retina homogenates. The minor presence of visual arrestin in RPE homogenates might be due to outer segment phagocytosis.

For each homogenate, four hemi-retinas or hemi-RPE were pooled and homogenized in 150 µl of a buffer containing 10 mM HEPES, 1 mM EDTA, 1 mM EGTA, 10 mM KCl, Triton 0.5% (v/v), pH 7.9, supplemented with a cocktail of protease inhibitors (Sigma Chemical Co. St. Louis, MO, USA). After 15 min at 4°C, homogenates were gently vortexed for 15 seconds and centrifuged at 900g for 10 min. Protein content was determined by the method of Lowry et al. (1951), using bovine serum albumin as the standard. Proteins (50 µg/sample) were separated in SDS, 12% polyacrylamide gel. After electrophoresis, proteins were transferred to polyvinylidenedifluoride membranes for 60 min at 15 V in a Bio-Rad Trans-Blot SD system (Bio-Rad Laboratories, Hercules, CA, USA). Membranes were blocked in 5% non-fat dry milk in Tris-buffered saline (pH 7.4), containing 0.1% Tween-20 for 60 min at room temperature and then incubated overnight at 4ºC with the primary antibodies. The following antibodies were used: a mouse monoclonal anti-complex IV (1:300, Invitrogen, Carlsbad, CA, USA), a mouse monoclonal anti-cytochrome c (1:1000, Santa Cruz Biotechnology, Dallas TX, USA), a rabbit polyclonal anti-traslocase of the outer membrane (TOM20, 1:500, Santa Cruz Biotechnology, Dallas TX, USA), a rabbit polyclonal anti-voltage-dependent selective-anion channel (VDAC) (1:300, Santa Cruz Biotechnology, Dallas, TX, USA), a rabbit polyclonal anti-heme oxygenase-1 (HO-1) (1:1000, Enzo Life Sciences, Farmingdale, NY, USA), a mouse monoclonal anti-superoxide dismutase-1 (SOD-1) (1:1000, Santa Cruz Biotechnology, Dallas, TX, USA), a mouse monoclonal anti-superoxide dismutase-2 (SOD-2) (1:1000, Santa Cruz Biotechnology, Dallas, TX, USA), a goat polyclonal anti-catalase (1:400, R&D Systems, Minneapolis, MN, USA), a mouse monoclonal anti-glutathione peroxidase (GPx) (1:1000, Santa Cruz Biotechnology, Dallas, TX, USA), a mouse anti- RPE65 (1:1000, EMD Millipore, Darmstadt, Germany), a mouse anti-visual arrestin (1:1000, Santa Cruz Biotechnology, Dallas, TX, USA), and a mouse anti-β-actin (1:1000, Santa

Cruz Biotechnology, Dallas, TX, USA). Membranes were washed and then incubated for 1 h with a horseradish peroxidase-conjugated secondary antibody. The following secondary antibodies were used: a donkey anti-mouse (1:2000, Jackson Laboratory, Bar Harbor, ME, USA), a donkey anti-rabbit (1:2000, Jackson Laboratory, Bar Harbor, ME, USA), and a donkey anti-goat (1:2000, Jackson Laboratory, Bar Harbor, ME, USA). Immunoblots were visualized by enhanced chemiluminescence Western blotting detection reagents (Amersham Biosciences, Buenos Aires, Argentina). Densitometric signals were quantified using ImageQuant software and adjusted by the density of β-actin. For each group, the mean of 6 homogenates were averaged and taken as the representative value.

***Ex vivo* flat-mounted RPE viability assessment**

After cervical dislocation, eyes were immediately enucleated, and RPE flat-mounts were obtained and incubated in a 1 μg/ml solution of propidium iodide (Sigma Aldrich, Saint Louis, MO, USA) and 1 μg/ml Hoechst (Sigma Chemical Co., St Louis, MO, USA) in mammalian Ringer (MR) buffer (157 mM NaCl, 5 mM KCl, 7 mM Na_2HPO_4, 8 mM NaH_2PO_4, 0.5 mM $MgCl_2$, 2 mM $CaCl_2$, pH 6.9) for 15 minutes at 37ºC. After several washes with fresh MR, samples were fixed in 4% paraformaldehyde for 10 minutes, washed in MR, mounted with fluorescent medium. Cells were considered viable at the nasal and temporal RPE flat-mounts when propidium iodide staining was absent in most Hoechst stained nuclei, as shown in Figure S2.

***Ex vivo* RPE mitochondrial labelling and superoxide detection**

RPE flat-mounts were obtained as described above and incubated with 500 nM MitoTracker Red CMXRos (Molecular Probes, Eugene, OR, USA) in MR buffer for 15 minutes or 5 μM MitoSOX Red (Molecular Probes, Eugene, OR, USA) in MR buffer for 30 minutes at 37ºC in

dim red light. After several washes in MR, samples were incubated with 1 μg/ml Hoechst (Sigma Chemical Co., St Louis, MO, USA), washed, fixed in 4% paraformaldehyde, mounted with fluorescent medium, and viewed under an epifluorescent microscope (BX-50, Olympus, Tokyo, Japan). For each group, 3 images from the nasal and temporal central RPE from 4 different eyes were analysed.

Immunofluorescence studies

Antigen retrieval was performed by heating slices at 90°C for 30 minutes in citrate buffer (pH 6.3). Sections were immersed in 0.1% Triton X-100 (Roche Diagnostics GmbH, Mannheim, Germany) in 0.1 mol L-1 PBS for 20 minutes for permeabilization. Sections were preincubated with 5% normal horse serum for 1 hour and then were incubated overnight at 4°C with primary antibodies. The following primary antibodies were used: a mouse monoclonal anti-SOD-1 (1:50, Santa Cruz Biotechnology, Dallas, TX, USA), a mouse monoclonal anti-SOD-2 (1:50, Santa Cruz Biotechnology, Dallas, TX, USA), a goat polyclonal anti-catalase (1:50, R&D Systems, Minneapolis, MN, USA), a mouse monoclonal anti-GPx (1:50, Santa Cruz Biotechnology, Dallas, TX, USA), a mouse monoclonal anti-4-hydroxy-2-nonenal (4HNE) (1:250, R&D Systems, Minneapolis, MN, USA), a mouse monoclonal anti-carboxymethyl-lysine (CML) (1:250, R&D Systems, Minneapolis, MN, USA), and a rabbit polyclonal anti-nuclear factor erythroid-2 related factor 2 (Nrf2) (1:100, Novus Biologicals, Littleton, CO, USA). After several washes, secondary antibodies were added, and sections were incubated for 2 h at room temperature. Regularly, some sections were treated without the primary antibodies to confirm specificity. The following secondary antibodies were used: a goat anti-mouse IgM conjugated to Alexa 568 (1:500; Invitrogen, Molecular Probes, Carlsbad, CA, USA), a goat anti-mouse IgM conjugated to Alexa 488 (1:500; Invitrogen, Molecular Probes, Carlsbad, CA, USA), a goat anti-rabbit IgM conjugated to Alexa 568 (1:500; Invitrogen, Molecular Probes, Carlsbad, CA, USA),

and a donkey anti-goat IgG conjugated to Alexa 488 (1:500; Abcam, Buenos Aires, Argentina). Nuclei were stained with Hoechst (1 μg/ml, Sigma Chemical Co., St Louis, MO, USA), mounted with fluorescent mounting medium and observed under an epifluorescence microscope (BX-50, Olympus, Tokyo, Japan) mounted with a video camera (3CCD; Sony, Tokyo, Japan) attached to a computer running image analysis software (Optimus, Media Cybernetics, Silver Spring, MD, USA). Comparative digital images from different samples were grabbed using identical time exposition, brightness, and contrast settings. Images from the nasal and temporal RPE and retina at 800 μm from the ONH were analysed. The mean of 4 eyes per group were averaged and taken as the representative value.

Superior cervical ganglionectomy

A ventral midline incision was made in the neck and the left superior cervical ganglion (SCG) was removed aseptically, as previously described (Dieguez et al., 2018; Romeo et al., 1991). This manoeuvre produces complete and permanent loss of ipsilateral orbital sympathetic innervation. Care was taken to avoid carotid artery tears. Incision was closed with 7-0 nylon sutures. All mice recovered without any sign of distress. A sham procedure, without removing the right SCG was performed, and the right eye was further then considered the control eye. In some animals, while the contralateral side remained intact, a sham procedure was performed without excision of the left SCG. In these animals, the right eye was called naïve. All animals were randomized before any experimental procedure was done and all investigators involved were blind to treatment.

Morphometric Analysis

All the images obtained were assembled and processed using Adobe Photoshop SC (Adobe Systems, San Jose, CA) to adjust the brightness and contrast. No other adjustments were made.

For all morphometric image processing and analysis, digitalized captured TIFF images were transferred to ImageJ software version 1.42q (NIH, Bethesda, MD). The analysers were masked for treatment and time point in all experiments.

Statistical analysis

Statistical analysis of results was made by a Student's t-test or a two-way analysis of variance (ANOVA) followed by a Tukey´s test, as stated, and met the necessary assumptions. The assumption of equal variances was tested by the F-test. In every statistical analysis $P<0.05$ was considered statistically significant.

RESULTS

Figure 1 shows representative photomicrographs and ultraphotomicrographs of the nasal and temporal RPE from intact eyes. Melanin content and melanosome granules number were significantly lower, and basal infoldings thickness was significantly higher at the temporal than at the nasal RPE. The analysis of mitochondria distribution (assessed with MitoTracker Red), intrinsic mitochondrial protein levels, and mitochondrial structure is shown in Figure 2. The number of MitoTracker Red(+) mitochondria and the levels of complex IV, cytochrome c, TOM20, and VDAC were significantly higher at the temporal than at the nasal RPE. A similar profile was observed for mitochondria area (Figure 2). The levels and localization of antioxidant enzymes in RPE from naïve eyes were analysed by Western blot and immunohistochemistry. Catalase, SOD-1, SOD-2, and GPx levels were significantly higher at the temporal than at the nasal RPE (Figure 3). These results were confirmed by immunohistochemistry, as also shown in Figure 3. No differences regarding antioxidant enzimes levels were observed between the nasal and temporal neural retina from naïve eyes (Figure S3). In order to analyse the effects of SCGx on the RPE endogenous antioxidant system, catalase, SOD-1, SOD-2, and GPx levels were

assessed by Western blot and immunohistochemistry (Figure 4). At 6 weeks post-surgery, SCGx induced a significant decrease in these parameters at the temporal (but not nasal) RPE (Figure 4). SCGx did not affect antioxidant enzimes levels in the nasal and temporal neural retina (Figure S4). SCGx induced an increase in 4HNE- and CML-immunostaining at the temporal (but not nasal) RPE and photoreceptor outer segments, and RPE, respectively. To reveal mitochondria superoxide production, RPE flat-mounts were incubated with MitoSOX probe. At 6 weeks post-SCGx, an increased number of MitoSOX-labelled mitochondria were observed at the temporal (but not nasal) RPE (Figure 5). Moreover, SCGx induced Nrf2 translocation to the nucleus and a significant increase in HO-1 levels only in the temporal RPE, as also shown in Figure 5. No differences in the levels and localization of 4HNE, CML, Nrf2, and HO-1 were observed between nasal and temporal retina from naïve, sham- or, SCGx-treated animals (data not shown). SCGx induced a significant decrease in MitoTracker-labelled mitochondria circumscribed to the temporal RPE (Figure 6). Moreover, SCGx significantly decreased complex IV, cytochrome c, TOM20, and VDAC levels only at the temporal RPE (Figure 6). Mitochondria ultrastructure was analysed in ultrathin sections from the RPE. At the temporal RPE, SGCx induced a significant decrease in mitochondria area, and frequent mitochondria ultrastructural alterations, such as membrane ruptures and electron dense material leak to the cytosol (Figure 6). No differences in any parameter studied were observed between the nasal and temporal side from naïve and sham-treated eyes (data not shown).

DISCUSSION

For the first time, the foregoing results demonstrate significant differences in melanin content, basal infoldings thickness, mitochondrial mass, and the antioxidant defensive system between the temporal and the nasal RPE from naïve C57BL/6J mice. In addition, the present results show that SCGx, that mimics cardinal features of NE-AMD (Dieguez et al., 2018), induced a decrease

in the mitochondrial mass and the endogenous antioxidant system, leading to ROS accumulation and oxidative damage circumscribed to the temporal RPE. Notably, this particular retinal region correlates with the central retinal area described by Volland and co-workers (2015). It has been shown that melanin content is lowest in the central retina from monkeys and dogs (Durairaj et al., 2012), and in the macula from human donors, regardless of their age (Durairaj et al., 2012; Schmidt and Peisch, 1986). In agreement, melanin content and melanosome granule number were significantly lower at the temporal than the nasal RPE from naïve C57BL/6J mice, suggesting another feature in common between the RPE at the human macula and the central temporal RPE in C57BL/6J mice. Since C57BL/6J mouse central retina might share some similarities with the human macula, which has a high metabolic rate (Datta et al., 2017), we studied the nasal and temporal RPE mitochondria by measuring the levels of different intrinsic mitochondrial proteins. Increased levels of complex IV, cytochrome c, TOM20 and VDAC, as well as MitoTracker-labelled mitochondria, and mitochondrial area were found in the temporal RPE from naïve mice, supporting a higher metabolic activity in the temporal than in the nasal RPE. ROS are produced by a variety of pathways of aerobic metabolism; however, the major source of their production is the mitochondria. As in other tissues, ROS coming from RPE mitochondria metabolism need to be efficiently detoxified. The endogenous antioxidant system includes the catalysis of superoxide anions to hydrogen peroxide by SOD, the degradation of hydrogen peroxide by catalase, and the reduction of ROS by glutathione *via* GPx. As shown herein, the levels of these antioxidant enzymes were significantly higher at the temporal than at the nasal RPE. Taken together, these results could suggest that the temporal RPE has evolved an increased metabolic activity likely to fulfil the local energetic demand, and a highly effective cytoprotective system to neutralize unwanted oxidative damage.

Since NE-AMD is characterized by a precise localization affecting the central retina, it is reasonable to think that the RPE, which displays histological, ultrastructural, and metabolic

differences between the nasal and temporal side (particularly at mitochondrial level), could show a differential regional susceptibility for damage provoked by SCGx-induced NE-AMD. Therefore, we studied the effect of SCGx on the mitochondrial status in the mouse nasal and temporal RPE. SCGx induced a significant decrease in SOD-1, SOD-2, catalase, and GPx levels at the temporal (but not nasal) RPE, which could lead to an increase in oxidative damage, supported by the increase in oxidized molecules (i.e., 4HNE and CML), and an increased number of MitoSOX-labelled mitochondria. Nrf2 is a transcriptional factor that that regulates the response to environmental stress and controls anti-oxidative responses and phase 2 enzymes such as HO-1 (Laboda et al., 2016). In agreement, increased nuclear levels of Nrf2 correlated with higher levels of HO-1 in the temporal RPE. Despite having high nuclear Nrf2 and HO-1 levels, this pathway seemed to be insufficient to protect the central temporal RPE, which showed signs of oxidative damage in SCGx-treated eyes. Echoed with our results, it has been demonstrated an increase in nuclear Nrf2-immunolabeling in the macular RPE from patients with early AMD (Datta et al., 2017). Several lines of evidence have implicated oxidative stress-induced damage to the RPE in the pathogenesis of NE-AMD (Datta et al., 2017; Hanus et al., 2015; Lambros and Plafker, 2016). In harmony with our findings, it has been shown that reduction in SOD-2 specifically in the RPE leads to some of the features of GA in mice (Mao et al., 2014), and that under oxidative stress conditions, RPE cells from AMD patients produce more ROS than those derived from normal donors (Golestaneh et al., 2017), and are unable to increase the expression of SOD during oxidative stress (Hyttinen et al., 2018; McCord and Edeas, 2005). The key role of RPE mitochondria is also supported by the demonstration that their damage is sufficient to cause photoreceptor death (Zhao et al., 2011), and injury induced by human AMD (Brown et al., 2018; Terluk et al., 2015). The fact that mitochondria are the major site of ROS production has led to the suggestion that mitochondria might be a prime target of oxidative damage (Van Remmen and Richardson, 2001). In this line, SCGx decreased temporal RPE mitochondrial mass, as shown by

a decrease in complex IV, cytochrome c, TOM20, VDAC, MitoTracker-labelled mitochondria, and mitochondria area. Electron micrograph studies demonstrate that aged individuals have fewer and smaller RPE mitochondria, and mitochondria depletion is even more severe in AMD patients whom in addition, have pronounced damage to mitochondrial structure and show displaced mitochondria (Feher et al., 2006; Karunadharma et al., 2010). Another study shows severe disruptions in mitochondrial inner and outer membrane structure and mitochondrial cellular organization, as well as mitochondrial smaller size in RPE from patients with NE-AMD (Brown et al., 2018). In agreement, SCGx induced ultrastructural mitochondria alterations at the temporal (but not nasal) RPE. Among other important functions, RPE cells are required for photoreceptor outer segment membrane phagocytosis, and therefore, critical for photoreceptor survival, function and renewal. Consequently, RPE degeneration caused by oxidative stress or other stresses usually causes secondary photoreceptor cell death. In agreement, we have shown photoreceptor apoptosis in the temporal retina at later stages of SCGx (i.e, at 10 weeks post-surgery) (Dieguez et al., 2018). Based on the present results, we could hypothesize that SCGx could downregulate the endogenous antioxidant defensive system in the temporal RPE resulting in oxidative damage, which in turn, could provoke a circumscribed RPE and photoreceptor damage. It remains unclear whether the observed phenomena are a factor contributing to disease progression or simply a result of disease. However, it should be noted that mitochondrial alterations induced by SCGx were observed at early stages of experimental NE-AMD (i.e., at 6 weeks post-surgery), which preceded RPE and photoreceptor apopotosis (Dieguez et al., 2018). These findings suggest that mitochondrial dysfunctions might be involved in the pathogenesis of NE-AMD, and therefore, mitochondria appear to be an important target for the survey of NE-AMD pathology, and possibly for providing promising therapeutic targets.

Despite no differences regarding mitochondrial status and antioxidant defensive system were observed between the nasal and temporal neural retina from naïve or ganglionectomized mice,

the present results could allow shedding light on one of the key and still unsolved questions of NE-AMD, which is why the human macula (but not the peripheral retina) is susceptible to degeneration. The present results support that the temporal RPE might be biochemically adapted to surpass oxidative stress, and that SCGx, which diminished only the temporal RPE antioxidant activity, induced a circumscribed damage at the temporal central region. Moreover, we have previously shown that sympathetic choroid denervation, which induces ubiquitous choroid alterations, only damages the temporal outer retina (Dieguez et al., 2018). Thus, despite the well-known differences between the human and mouse retina, it is tempting to speculate that it might not be the pathophysiology of NE-AMD which conditions the localization of the disease, but the macular RPE histologic and metabolic specific attributes that make it more susceptible to choroid alterations leading initially to a localized RPE dysfunction/damage, and secondarily to macular degeneration.

FUNDING

This work was funded by the National Scientific and Technical Research Council (CONICET) PIP 0707, the National Agency for Scientific and Technical Promotion (ANPCYT) PICT 1563, PICT 0356, and PICT 2731, the University of Buenos Aires (UBA) 20020100100678.

REFERENCES:

Ach T, Tolstik E, Messinger JD, Zarubina AV, Heintzmann R, Curcio CA (2015) Lipofuscin redistribution and loss accompanied by cytoskeletal stress in retinal pigment epithelium of eyes with age-related macular degeneration. *Invest Ophthalmol Vis Sci* 56: 3242-3252.

Bowes Rickman C, Farsiu S, Toth CA, Klingeborn M (2013) Dry age-related macular degeneration: mechanisms, therapeutic targets, and imaging. *Invest Ophthalmol Vis Sci* 54:ORSF68-80.

Brown EE, Lewin AS, Ash JD (2018) Mitochondria: Potential Targets for Protection in Age-Related Macular Degeneration. *Adv Exp Med Biol* 1074:11-17.

Buschini E, Fea AM, Lavia CA, Nassisi M, Pignata G, Zola M, Grignolo FM (2015) Recent developments in the management of dry age-related macular degeneration. *Clin Ophthalmo*l 9: 563-574.

Cai J, Nelson KC, Wu M, Sternberg P, Jr, Jones DP (2000) Oxidative damage and protection of the RPE. *Prog Retin Eye Res* 19:205-221.

Datta S, Cano M, Ebrahimi K, Wang L, Handa JT (2017) The impact of oxidative stress and inflammation on RPE degeneration in non-neovascular AMD. *Prog Retin Eye Res* 60: 201-218.

Dieguez HH, Romeo HE, González Fleitas MF, Aranda ML, Milne GA, Rosenstein RE, Dorfman D (2018) Superior cervical gangliectomy induces non-exudative age-related macular degeneration in mice. *Dis Model Mech* 11(2). pii: dmm031641. doi: 10.1242/dmm.031641.

Ding X, Patel M, Chan CC (2009) Molecular pathology of age-related macular degeneration. *Prog Retin Eye Res* 28:1-18.

Durairaj C, Chastain JE, Kompella UB (2012) Intraocular distribution of melanin in human, monkey, rabbit, minipig and dog eyes. *Exp Eye Res* 98: 23-27.

Feher J, Kovacs I, Artico M, Cavallotti C, Papale A, Balacco Gabrieli C (2006) Mitochondrial alterations of retinal pigment epithelium in age-related macular degeneration. *Neurobiol Aging* 27: 983-993.

Golestaneh N, Chu Y, Xiao YY, Stoleru GL, Theos AC (2017) Dysfunctional autophagy in RPE, a contributing factor in age-related macular degeneration. *Cell Death Dis* 8: e2537.

Jager RD, Mieler WF, Miller JW (2008) Age-related macular degeneration. *N Engl J Med* 358:2606-2617.

Hanus J, Anderson C, Wang S (2015) RPE necroptosis in response to oxidative stress and in AMD. *Ageing Res Rev* 24:286-298.

Hyttinen JMT, Viiri J, Kaarniranta K, Błasiak J (2018) Mitochondrial quality control in AMD: does mitophagy play a pivotal role? *Cell Mol Life Sci* doi: 10.1007/s00018-018-2843-7.

Karunadharma PP, Nordgaard CL, Olsen TW, Ferrington DA (2010) Mitochondrial DNA damage as a potential mechanism for age-related macular degeneration. *Invest Ophthalmol Vis Sci* 51: 5470-5479.

Laboda A, Damulewicz M, Pyza E, Jozkowicz A, Dulak J (2016) Role of Nrf2/HO-1 system in development, oxidative stress response and diseases: an evolutionarily conserved mechanism. *Cell Mol Life Sci* 17:3221-47.

Lambert NG, ElShelmani H, Singh MK, Mansergh FC, Wride MA, Padilla M, Keegan D, Hogg RE, Ambati BK (2016) Risk factors and biomarkers of age-related macular degeneration. *Prog Retin Eye Res* 54: 64-102.

Lambros ML, Plafker SM (2016) Oxidative Stress and the Nrf2 Anti-Oxidant Transcription Factor in Age-Related Macular Degeneration. *Adv Exp Med Biol* 854: 67-72.

Lowry OH, Rosebrough NJ, Farr AL, Randall RJ (1951) Protein measurement with the Folin phenol reagent. *J Biol Chem* 193:265-275.

Mao H, Seo SJ, Biswal MR, Li H, Conners M, Nandyala A, Jones K, Le YZ, Lewin AS (2014) Mitochondrial oxidative stress in the retinal pigment epithelium leads to localized retinal degeneration. *Invest Ophthalmol Vis Sci* 55: 4613-4627.

McCord JM, Edeas MA (2005) SOD, oxidative stress and human pathologies: a brief history and a future vision. *Biomed Pharmacother* 59:139-142.

Romeo HE, Colombo LL, Esquifino AI, Rosenstein RE, Chuluyan HE, Cardinali DP (1991) Slower growth of tumours in sympathetically denervated murine skin. *J Auton Nerv Syst* 32:159-164.

Sachdeva MM, Cano M, Handa JT (2014) Nrf2 signaling is impaired in the aging RPE given an oxidative insult. *Exp Eye Res* 119:111-114.

Schmidt SY, Peisch RD (1986) Melanin concentration in normal human retinal pigment epithelium. Regional variation and age-related reduction. *Invest Ophthalmol Vis Sci* 27:1063-1067.

Terluk MR, Kapphahn RJ, Soukup LM, Gong H, Gallardo C, Montezuma SR, Ferrington DA (2015) Investigating mitochondria as a target for treating age-related macular degeneration. *J Neurosci* 35:7304-7311.

van Lookeren Campagne M, LeCouter J, Yaspan BL, Ye W (2014) Mechanisms of age-related macular degeneration and therapeutic opportunities. *J Pathol* 232:151-164.

Van Remmen H, Richardson A (2001) Oxidative damage to mitochondria and aging. *Exp Gerontol* 36: 957-968.

Volland S, Esteve-Rudd J, Hoo J, Yee C, Williams DS (2015) A comparison of some organizational characteristics of the mouse central retina and the human macula. *PLoS One* 10: e0125631. doi: 10.1371/journal.pone.0125631.

Winkler BS, Boulton ME, Gottsch JD, Sternberg P (1999) Oxidative damage and age-related macular degeneration. *Mol Vis* 5: 32-58.

Wong WL, Su X, Li X, Cheung CM, Klein R, Cheng CY, Wong TY (2014) Global prevalence of age-related macular degeneration and disease burden projection for 2020 and 2040: a systematic review and meta-analysis. *Lancet Glob Health* 2: 106-116.

Zarbin MA (2004) Current concepts in the pathogenesis of age-related macular degeneration. *Arch Ophthalmol* 122: 598-614.

Zhao C, Yasumura D, Li X, Matthes M, Lloyd M, Nielsen G, Ahern K, Snyder M, Bok D, Dunaief JL, LaVail MM, Vollrath D (2011) mTOR-mediated dedifferentiation of the retinal pigment epithelium initiates photoreceptor degeneration in mice. *J Clin Invest* 121:369-383.

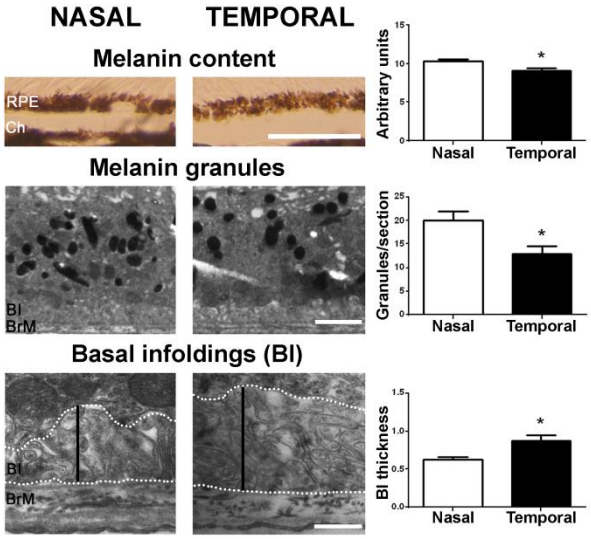

Figure 1. Histological differences between the nasal and temporal RPE from naïve mice. Upper panel: Transverse sections from the central nasal and temporal RPE (at 800 μm from the ONH). Melanin content was significantly lower at the temporal RPE. Middle and lower panel: Ultrathin sections of the RPE at 800 μm from the ONH. The number of melanin granules was significantly lower, whereas basal infoldings were significantly thicker (black bars) at the temporal RPE. Shown are photomicrographs representative from 5 eyes. RPE, retinal pigment epithelium; BrM, Bruch´s membrane; BI, basal infoldings. Scale bar upper panel = 25 μm, middle panel = 2 μm, lower panel = 200 nm. Data are mean ± SEM (n: 5 eyes per group), **P* < 0.05 vs. nasal RPE, by Student´s t-test.

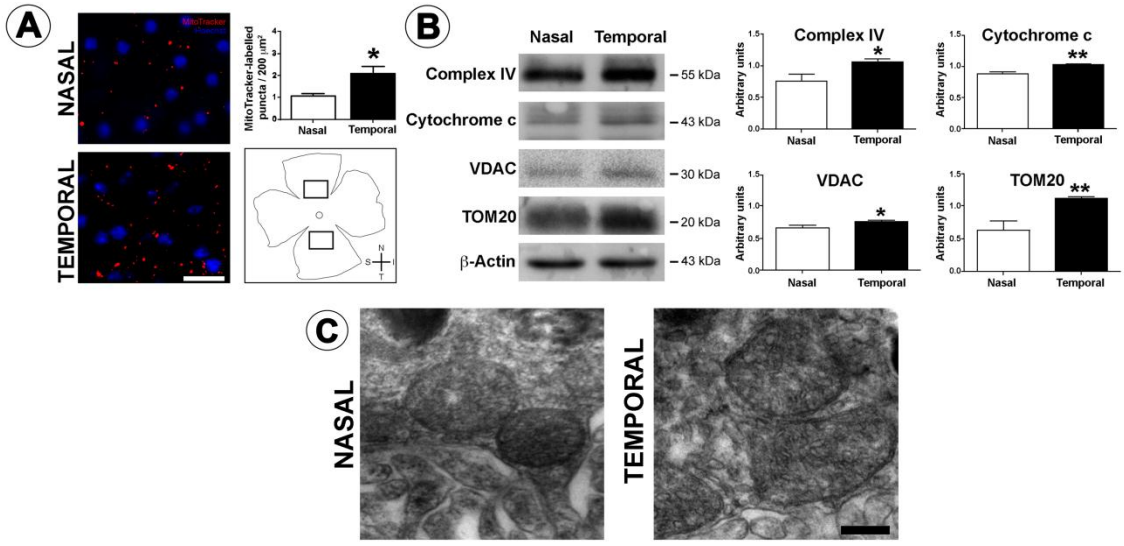

Figure 2. Region-specific mitochondria mass differences in the RPE from naïve mice. Panel A: Mitotracker-Red-labeled mitochondria at the central nasal and temporal RPE flat-mounts. The number of Mitotracker-Red(+) puncta was significantly higher at the temporal RPE. Shown are photomicrographs representative from 4 eyes. Data are mean ± SEM (n: 4 eyes per group), $*P < 0.05$ vs. nasal RPE, by Student´s t-test. Panel B: Representative *Western blot* analysis for mitochondria specific proteins from the nasal and temporal RPE. Complex IV, cytochrome c, VDAC, and TOM20 levels were significantly higher at the temporal than at the nasal RPE. Densitometric analysis is shown on the right. Data are mean ± SEM (n: 6 samples per group), $**P < 0.01$, $*P < 0.05$ vs. nasal RPE, by Student´s t-test. Panel C: Mitochondria analysis on ultrathin sections of the central nasal and temporal RPE. The mitochondria area was significantly higher at the temporal RPE. Shown are photomicrographs representative from 5 eyes. Data are mean ± SEM (n: 5 eyes per group),$*P < 0.05$ vs. nasal RPE, by Student´s t-test. Scale bar panel A = 50 µm, panel C = 400 nm.

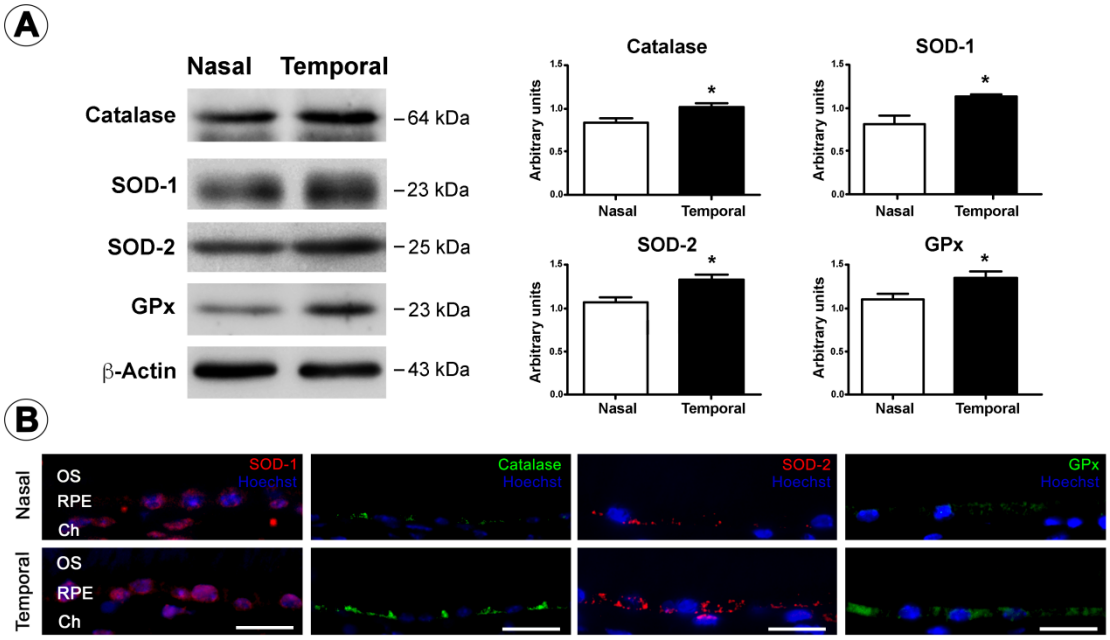

Figure 3. Region-dependent antioxidant status in the RPE from naïve mice. Panel A: Representative *Western blots*. Catalase, SOD-1, SOD-2, and GPx levels were significantly higher at the temporal than at the nasal RPE. Densitometric analysis is shown on the right. Data are mean ± SEM (n: 6 samples per group), **P* < 0.05 vs. nasal RPE, by Student´s t-test. Panel B: Localization of nasal and temporal RPE antioxidant enzymes at 800 μm from the ONH. An increased SOD-1-, catalase-, SOD-2-, and GPx-immunoreactivity was observed at the temporal region. Shown are photomicrographs representative from 4 eyes. OS, photoreceptor outer segments; RPE, retinal pigment epithelium; Ch, choroid. Scale bars = 25 μm.

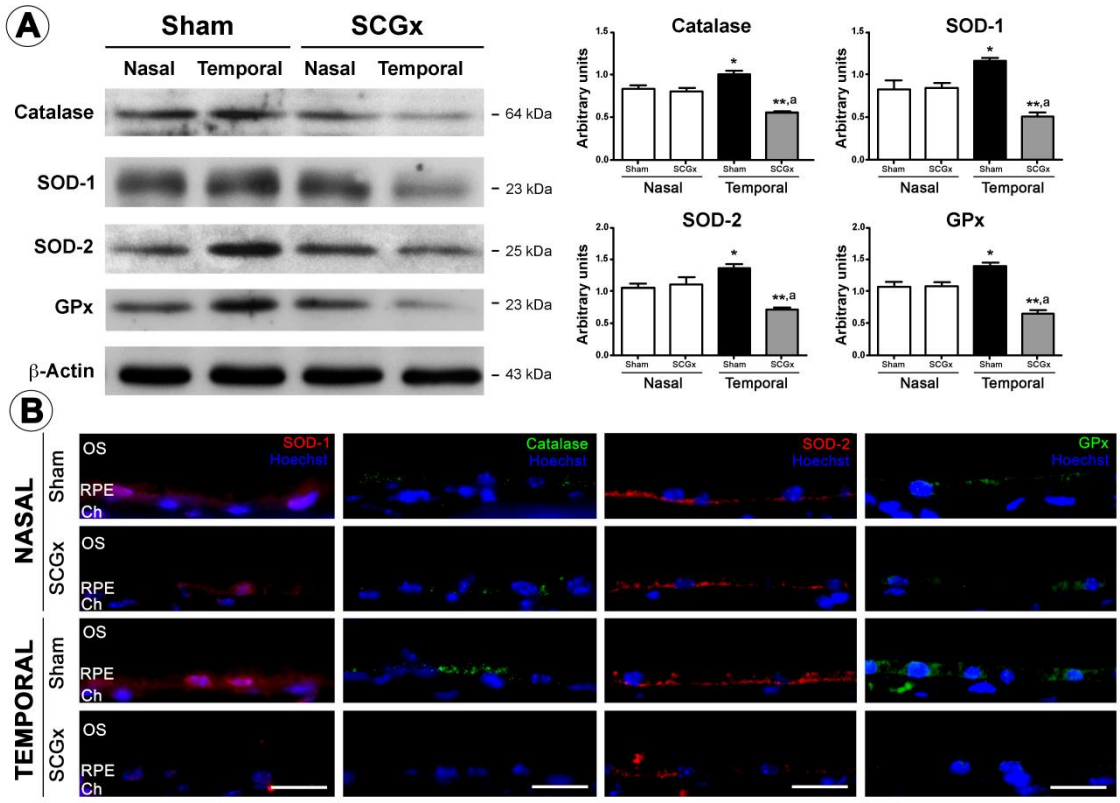

Figure 4. Region-dependent effect of SCGx on the RPE antioxidant system. Panel A: Representative *Western blots* for the assessment antioxidant enzyme levels at the nasal and temporal RPE from sham- or SCGx-treated eyes. Catalase, SOD-1, SOD-2, and GPx levels were significantly higher at the temporal than at the nasal sham-treated RPE, whereas SCGx, which had no effect on the nasal region, induced a significant decrease in antioxidant enzyme levels at the temporal RPE. Densitometric analysis is shown on the right. Data are mean ± SEM (n: 6 samples per group), $^{**}P < 0.01$, $^{*}P < 0.05$ vs. nasal RPE from sham-treated eyes; a*: $P < 0.01$* vs. temporal RPE from sham-treated eyes, by Tukey´s test (catalase F=36.0; SOD-1 F=31.7; SOD-2 F=27.07; GPx F=41.67). Panel B: Localization of SOD-1, catalase, SOD-2, and GPx at the nasal and temporal RPE at 800 μm from the ONH. SOD-1-, catalase-, SOD-2-, and GPx-immunoreactivity was higher at the temporal than at the nasal RPE from sham-treated eyes, while SCGx, which had no effect on the nasal region, induced a decrease in antioxidant enzyme immunoreactivity at the temporal side. Shown are photomicrographs representative from 4 eyes/group. OS, photoreceptor outer segments; RPE, retinal pigment epithelium; Ch, choroid. Scale bars = 25 μm.

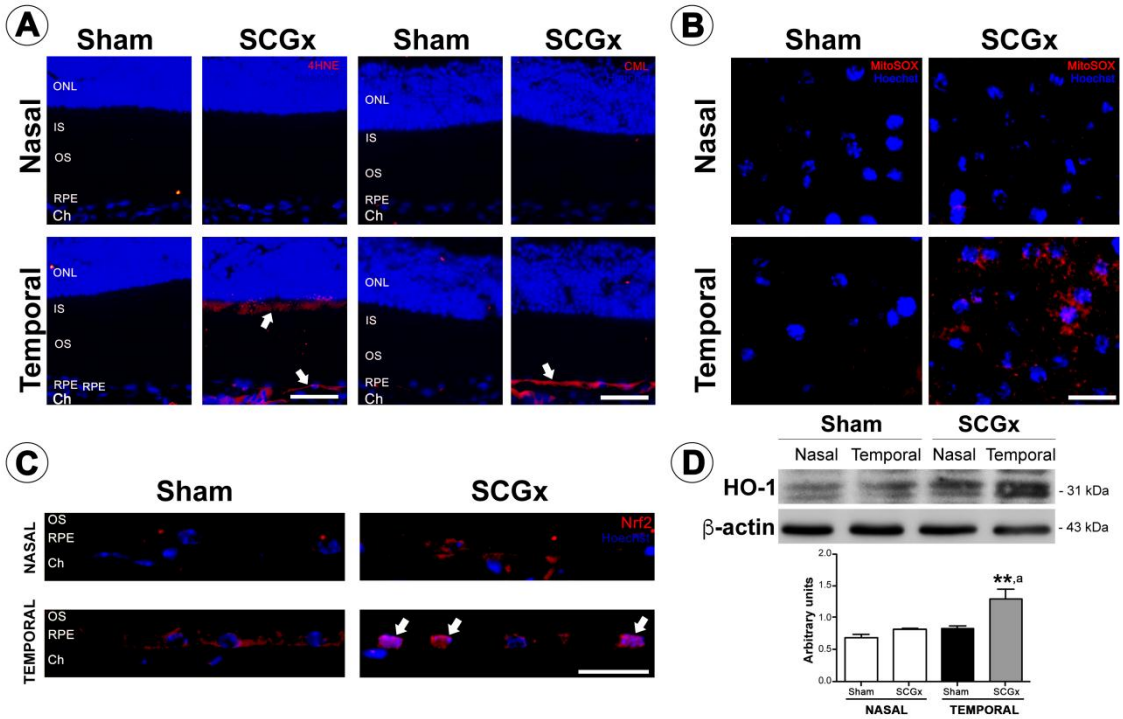

Figure 5. Region-dependent effect of SCGx on the RPE oxidative damage. Panel A: 4HNE- and CML-immunostaining at the nasal and temporal outer retina and RPE at 6 weeks post-SCGx. SGCx induced an increase in 4HNE- and CML-immunoreactivity at the temporal outer retina and RPE (arrows), and RPE respectively. Shown are photomicrographs representative from 6 eyes/group. Panel B: MitoSOX-labeled mitochondria at the central nasal and temporal RPE flat-mounts. SCGx induced the occurrence of MitoSOX(+) mitochondria only at the temporal RPE. Shown are photomicrographs representative from 4 eyes/group. Panel C: Localization of Nrf2 at the nasal and temporal RPE. SCGx induced Nrf-2 traslocation to the nucleus exclusively at the temporal RPE. Shown are photomicrographs representative from 4 eyes/group. Panel D: Representative *Western blot* for HO-1 assessment at the nasal and temporal RPE from sham- or SCGx-treated eyes at 6 weeks post-surgery. SCGx, which had no effect at the nasal region, induced a significant increase in HO-1 levels at the temporal region. Densitometric analysis is shown on the right. Data are mean ± SEM (n: 6 samples/ group), $^{**}P < 0.01$ vs. nasal RPE from sham-treated eyes; a: $P < 0.01$ vs. temporal RPE from sham-treated eyes, by Tukey´s test (F=4.53). ONL, outer nuclear layer; IS, photoreceptor inner segments; OS, photoreceptor outer segments; RPE, retinal pigment epithelium; Ch, choroid. Scale bars = 25 μm.

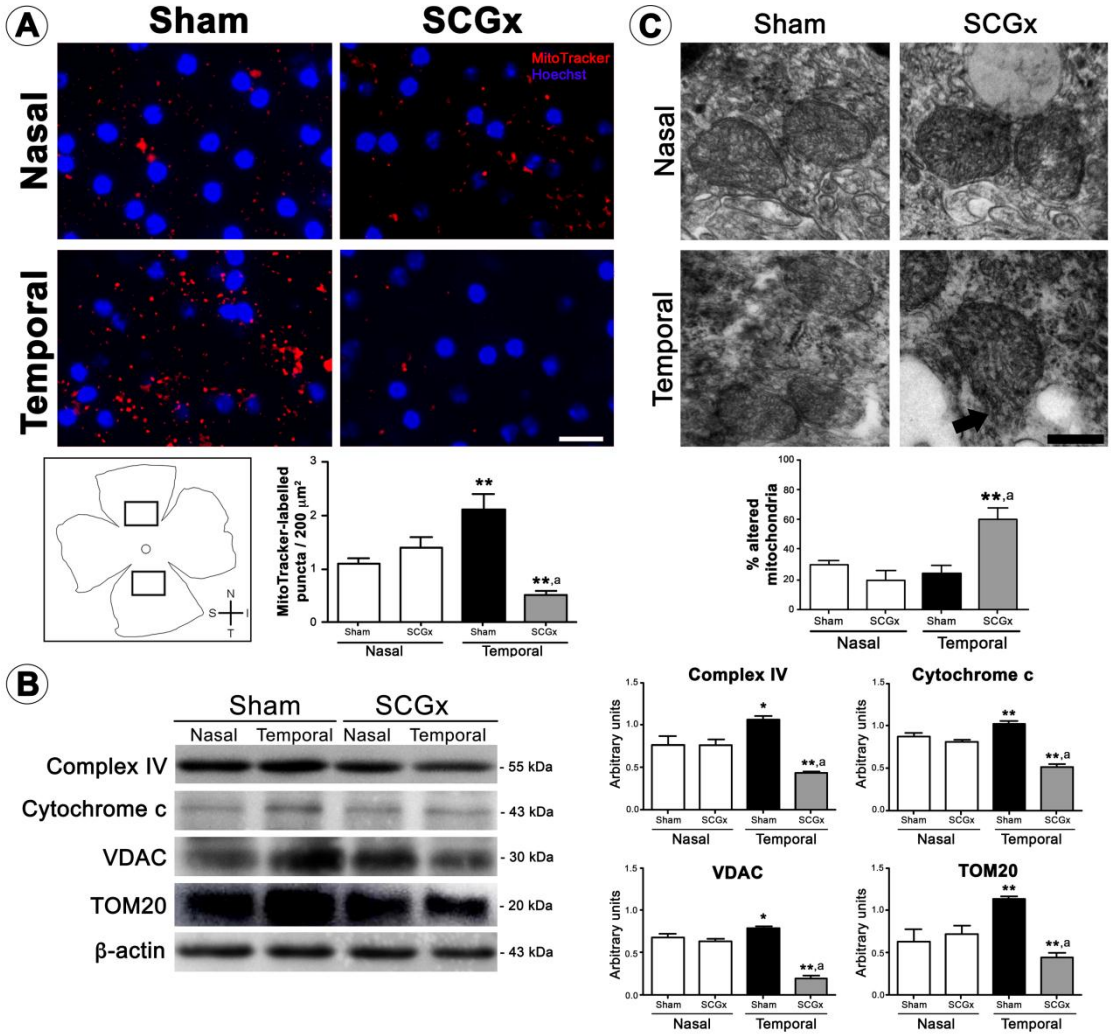

Figure 6. Region-dependent effect of SCGx on the RPE mitochondria mass. Panel A: Mitotracker-Red-labeled mitochondria in the central nasal and temporal RPE flat-mounts at 6 weeks post-SCGx. The number of Mitotracker-Red(+) puncta was significantly higher at the temporal sham-treated RPE, whereas SCGx induced a significant decrease in this parameter in the temporal region. Shown are photomicrographs representative from 4 eyes. Data are mean ± SEM (n: 4 eyes per group), $^{**}P < 0.01$ vs. nasal sham-treated RPE; a: $P < 0.01$ vs. temporal sham-treated RPE, by Tukey´s test (F=24.07). Panel B: Representative *Western blots* for the assessment of mitochondria intrinsic proteins. Complex IV, cytochrome c, VDAC, and TOM20 levels were significantly higher at the temporal RPE from sham-treated eyes. SCGx, which had no effect on the nasal RPE, induced a decrease in the levels of the temporal RPE mitochondria proteins. Densitometric analysis is shown on the right. Data are mean ± SEM (n: 6 samples per group), $^{**}P < 0.01$, $^{*}P < 0.05$ vs. nasal sham-treated RPE; a: $P < 0.01$ vs. temporal sham-treated RPE, by Tukey´s test (complex IV F=27.95; cytochrome c F=67.5; VDAC F=156.5; TOM20 F=20.88). Panel C: Mitochondria area on ultrathin sections of the nasal and temporal RPE at 800

μm from the ONH. Shown are photomicrographs representative from 5 eyes. Mitochondria area was significantly higher at the temporal side from sham-treated RPE, whereas SGCx induced a significant decrease in this parameter in the temporal region. Moreover, SGCx induced the occurrence of altered mitochondria at the temporal RPE. SCGx had no effects on both parameters at the nasal RPE. Data are mean ± SEM (n: 5 eyes per group), $^{**}P < 0.01$, $^{*}P < 0.05$ vs. nasal sham-treated RPE; a: $P < 0.01$ vs. temporal sham-treated RPE, by Tukey´s test (mitochondria area F=40.03; mitochondria damage F=26.56). Scale bar panel A = 50 μm, panel C = 400 nm.

HIGHLIGHTS:

- The temporal retinal pigment epithelium (tRPE) has lower melanin content.
- Higher antioxidant enzyme levels and mitochondria mass occur in the tRPE.
- Superior cervical ganglionectomy (SCGx) induces oxidative stress only in the tRPE.
- SCGx decreases mitochondria mass circumscribed to the tRPE.

Oxidative stress and mitochondria are key factors in early macular degeneration.

SUPPLEMENTARY FIGURE LEGENDS

Figure S1. Tissue homogenates specificity evaluation. Representative *Western blots* analyzing the presence of visual arrestin and RPE65 in retina and RPE lysates. While visual arrestin was highly present in retinal homogenates, and only marginally present in RPE lysates, RPE65 was only detected in RPE homogenates.

Figure S2. *Ex-vivo* flat-mounted RPE viability assessment. *Ex-vivo* RPE flat-mounts were incubated with propidium iodide. Shown are photomicrographs representative from 4 eyes. A low amount of propidium iodide(+) nuclei were observed at the central nasal and temporal RPE. Scale bar = 50 μm.

Figure S3. Region-dependent antioxidant status in the retina from naïve eyes. Representative *Western blots* for catalase, SOD-1, SOD-2, and GPx analysis at the nasal and temporal retina. There were no differences in the levels of catalase, SOD-1, SOD-2, and GPx

between the nasal and the temporal retina. Densitometric analysis is shown on the right. Data are mean ± SEM (n: 6 samples per group).

Figure S4. Region-dependent effect of SCGx on the retina antioxidant system. Representative *Western blots* for antioxidant enzymes analysis at the nasal and temporal retina from sham- or SCGx-treated eyes at 6 weeks post-surgery. There were no region-specific differences in the levels of catalase, SOD-1, SOD-2, and GPx in sham-treated retina, and SCGx had no effects on the levels of antioxidant enzymes. Densitometric analysis is shown on the right. Data are mean ± SEM (n: 6 samples per group).